Electrochemistry of a series of symmetric and asymmetric CpNiBr(NHC) complexes: Probing the electrochemical environment due to push-pull effects

Frederick P. Malan,[a] Eric Singleton,[a] Jeanet Conradie[b,*] and Marilé Landman[a,*]

[a] *Department of Chemistry, University of Pretoria, 02 Lynnwood Road, Hatfield, Pretoria, 0002, South Africa. E-mail: marile.landman@up.ac.za.*

[b] *Department of Chemistry, University of the Free State, Bloemfontein 9300, South Africa. E-mail: conradj@ufs.ac.za*

Graphical abstract

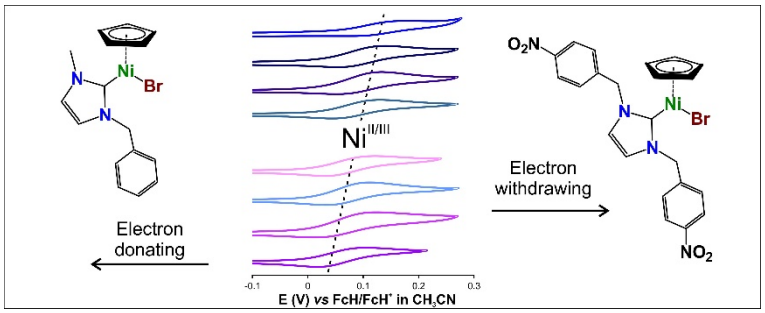

Synopsis

The electrochemistry of Ni(II) N-heterocyclic carbene complexes shows Ni^{II}/Ni^{III} oxidation, Ni^{II}/Ni^{I} reduction as well as NO_2-ligand based reduction.

Highlights

- Redox processes of [CpNiBr(NHC)] complexes are both metal and ligand-based
- Three oxidation states of Ni (I, II, III) are observed
- Oxidation of NO_2-containing complexes more positive relative to non-NO_2 analogues
- Redox data and DFT calculations confirm the centres associated with each process

Abstract

The electrochemistry of nine Ni(II) N-heterocyclic carbene (NHC) complexes of general formula [CpNiBr(NHC)], bearing either a symmetric or asymmetric *N*-substituted alkyl/benzyl/phenethyl NHC ligand with Cp = cyclopentadienyl is described. Both metal and ligand-centred redox processes have been observed and systematically evaluated. The reversible to quasi-reversible Ni^{II}/Ni^{III} couple (0.062 V ≤ $E^{0\prime}$ ≤ 0.127 V) is followed by the electrochemically and chemically irreversible ligand based oxidation peaks (E_{pa} ~ 0.37 V and ~0.5 V). The Ni^{II}/Ni^{I} and NHC ligand reduction processes were observed below -1.3 V. A comparison between the nine different Ni(II)-NHC complexes revealed that the electron-withdrawing NO_2-containing NHC ligands exhibit the most positive metal-oxidation redox processes. A DFT study complements the experimental findings by establishing where the oxidation and reduction centres were based.

Keywords:

nickel; cyclopentadienyl; *N*-heterocyclic carbene; electrochemistry; DFT

1. Introduction

Many of the catalytically active zero valent metal complexes employed in literature require ligands to assist in stabilising these sensitive species and preventing catalyst decomposition [1-5]. *N*-heterocyclic carbenes (NHCs) remain a favourite class of ancillary ligands that provides additional steric- and electronic ligand tuning options [3,5-12]. The stronger binding of NHCs to metal centres helps to avoid rapid degradation under oxidising conditions, as is the case with most common ligands [13,14]. Cyclopentadienyl nickel(II) halo complexes containing NHC ligands, [CpNiX(NHC)] (X = Cl, Br, I), have been actively studied by various research groups over the last two decades. Since their first reported synthesis by Cowley *et al.* [15] in 2000, this versatile class of complexes has been employed in numerous useful catalytic applications including Suzuki-Miyaura coupling reactions [16-18], Kumada-Tamao-Corriu coupling reactions [19], the hydrothiolation of alkynes [20], hydrosilylation of aldehydes and ketones [5], styrene [16] and phenylacetylene polymerisation reactions [21], Buchwald amination [22], secondary alcohol oxidation [11], α-arylation of ketones [23], dehalogenation reactions [24], as well as energy storage applications [25,26].

We have recently extended the existing limited range [21, 27 - 29] of [CpNiBr(NHC)] complexes to include bulky, flexible symmetric and asymmetric NHC ligands, which were found to be catalytically active for Suzuki-Miyaura coupling [30] and anaerobic secondary alcohol oxidation reactions [31]. Despite their versatile application possibilities, electrochemical studies on the redox properties of this class of [CpNiX(NHC)] (X = Cl, Br, I) complexes remain ill-explored. Only one report by Crabtree *et al.* [25] evaluates the preliminary electrochemical data of a series of six [CpNiX(NHC)] (X = Cl, I) complexes. The NHCs of their series contained a number of different substituents on the imidazolylidene backbone, including electron-withdrawing chlorido- and cyanido moieties, and a conjugated benzimidazole or a triazolidene ligand system. All complexes, in general, showed two or more, electrochemically irreversible oxidation features (large peak separations at a scan rate of 0.1 V s^{-1}), the first assigned to Ni^{II}/Ni^{III} oxidation. Only [CpNiCl(IMes)] (IMes = 1,3-bis(2,4,6-trimethylphenyl)imidazol-2-ylidene) showed a electrochemically reversible Ni^{II}/Ni^{III} oxidation. A quasi-reversible reduction was also observed for the latter complex at -1

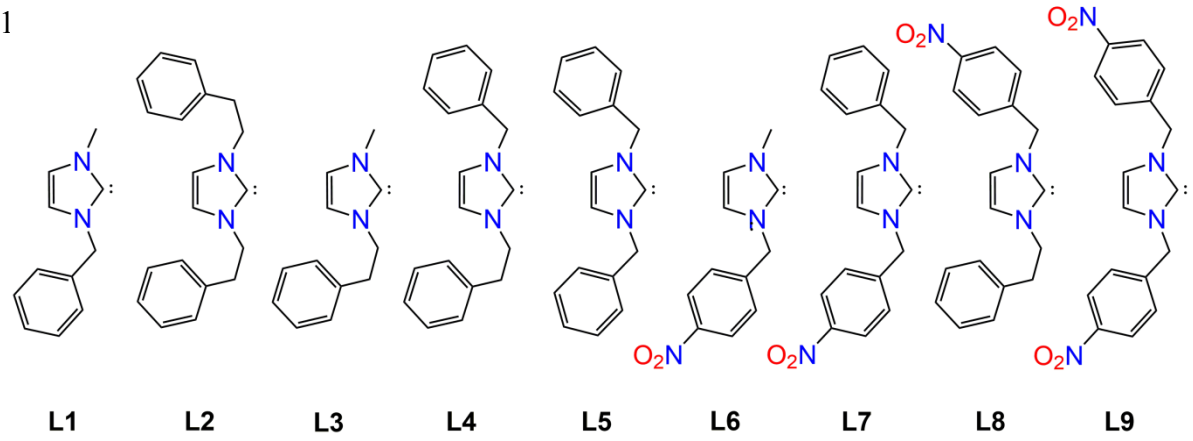

Figure 1: The ligands employed in the synthesis of the complexes [CpNiBr(NHC)] (**1**–**9**).

The main focus of this study is to investigate the effect of a series of unique NHC ligands featuring different *N*-substituents (see Figure 1) on the Ni^{II}/Ni^{III} redox couple of [CpNiBr(NHC)] (**1-9**), how it relates to the observed catalytic activity, and the determination of the locus of the observed redox processes by means of density functional theory (DFT) calculations. This study also correlates DFT calculated electronic energies from which linear relationships with the experimental electronic redox potentials were obtained.

2. Experimental

2.1 General

All experiments were carried out under an argon atmosphere using standard Schlenk techniques. Solvents were dried prior to use using standard techniques [32,33]. Column chromatography was carried out under inert argon atmospheres using silica gel (particle size 0.063-0.200 mm) as the stationary phase. The synthesis, purification, and characterisation of complexes [CpNiBr(NHC)] (**1-9**) (Figure 1) were performed as previously reported by our group [30]. All other chemicals were purchased from Sigma-Aldrich and used without further purification.

2.2 Electrochemistry

Cyclic voltammetry (CV), Osteryoung square wave voltammetry (OSWV) and linear sweep voltammetry (LSV) measurements were performed using 0.002 or saturated mol.dm^{-3} solutions of the complexes in dry acetonitrile (Aldrich, Biotech grade, 99.93% purity, anhydrous, kept under argon) containing 0.1 mol.dm^{-3} tetra-*N*-butylammonium hexafluorophosphate [NBu_4][PF_6] (Fluka, electrochemical grade) as supporting electrolyte under a purified argon atmosphere at 25 ºC. A three electrode cell, with a glassy carbon (surface area = 7.07 × 10^{-6} m^2) working electrode, a Pt auxiliary electrode, and a Ag/Ag$^+$ (0.010 mol.dm^{-3} $AgNO_3$ in CH_3CN) reference electrode mounted on a Luggin capillary, was used. Successive experiments under identical experimental conditions revealed all redox potentials were reproducible within 5 mV. All reported potentials were referenced against the IUPAC suggested FcH/FcH$^+$ couple. Ferrocene exhibited a formal reduction potential of $E^{0\prime}$ = 0.084 V *vs.* Ag/Ag$^+$, a peak separation of $\Delta E_p = E_{pa} - E_{pc}$ = 0.066 V, and i_{pa}/i_{pc} = 1.00, under our experimental conditions. E_{pa} (E_{pc}) = anodic (cathodic) peak potential and i_{pa} (i_{pc}) = anodic (cathodic) peak current. $E^{0\prime}$ (Fc/Fc$^+$) = 0.400 V *vs.* NHE. Decamethyl ferrocene (Fc*, -0.508 V *vs.* FcH/FcH$^+$) was used as internal standard. All linear sweep voltammogram (LSV) measurements were taken at a stationary electrode using a very slow scan rate of 2 mVs^{-1}. LSVs taken under slow scan rates have a sigmoidal shape and the limiting current is proportional to the analyte concentration [34]. The limiting current of different reduction and/or oxidation processes of the same sample can thus be quantitatively compared in terms of the relative amount of electron transferred during these processes.

2.3 Computational methods

All calculations were carried out using DFT with the B3LYP hybrid functional [35,36], and were implemented in the gas phase using the Gaussian 09 program [37]. The triple-ζ basis set 6-311G basis set was used for all atoms (C, H, N, Br, O), whereas the Stuttgart/Dresden (SDD) pseudopotential was used to describe the nickel and bromide electronic cores, while the metal valence electrons were described using the def2-TZVPP basis set [38]. All geometries were optimised without any symmetry restrictions, ensuring that the local minima had zero imaginary vibrational frequencies [39]. All of the redox processes involved one-electron transfer processes, and were therefore modelled as calculated electron affinities or ionisation potential, (EA)/(IP), defined as the amount of energy released/absorbed when an electron is added/removed from a neutral molecule. The adiabatic electron affinity (EA) and ionisation potential (IP) were calculated as the difference between the energy of the neutral complex (n electrons), and either the reduced (n + 1 electrons) or oxidised (n – 1 electrons) complexes, all at their respective optimised geometries. The neutral series of [CpNi(II)Br(NHC)] two-legged piano stool complexes were modelled as low spin diamagnetic (singlet multiplicity) d^8 complexes since the singlet calculations resulted in lower energies (0.09-0.12 eV) compared to triplet multiplicity calculations, for all complexes.

3. Results and Discussion

3.1 Synthesis of nickel(II) NHC complexes

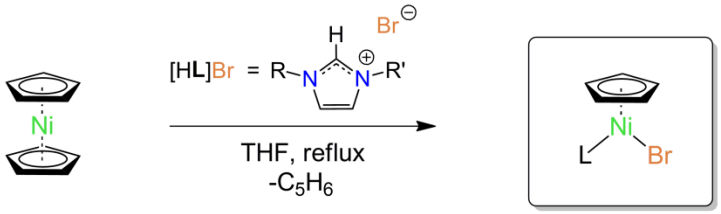

Figure 2: Synthetic route to the complexes [CpNiBr(NHC)] (**1-9**). L = NHC ligand with R and R' = Me (methyl), Bn (benzyl), $(CH_2)_2Ph$ (phenethyl) or 4-NO_2Bn (4-nitrobenzyl), as shown in Figure 1.

The synthesis and full characterisation of the range of investigated [CpNiBr(NHC)] complexes **1-9** containing flexible symmetric- and asymmetric NHC ligands, has been described in the literature [30,31]. The general synthesis involves the reflux of an anhydrous

THF slurry containing imidazolium bromide [HIm]Br and one equivalent of nickelocene ($NiCp_2$) for 3-16 hours (depending on the NHC salt), see Figure 2. The reaction mixture is then concentrated *in vacuo*, subjected to column chromatography (DCM/hexane), after which the collected red fraction was concentrated *in vacuo* to obtain red to red-brown powders [30]. Steric and electronic differences within each of these NHC ligands were incorporated by employing *N*-alkyl, -benzyl, and/or -phenethyl moieties, through which the resulting NHCs exhibited a degree of steric bulk and flexibility (Figure 1). The NO_2 group is introduced to reduce the electron donating ability of the NHC ligand and consequently the electron density on the coordinated nickel(II) ion for selected complexes; the NO_2 group is strongly electron withdrawing [40,41].

3.3 Electrochemistry

The cyclic voltammograms at a scan rate of 0.100 V s^{-1} of Ni(II)-NHC complexes **1-9** in the -1.8 V to +0.8 V *vs.* FcH/FcH^+ region are shown in Figure 3, along with a summary of the electrochemical data in Table 1. A graph of scan rates 0.05 – 5.00 V s^{-1} of the first oxidation peak for **5** is shown in Figure 4 (see Supplementary Information for more results). In the oxidation region, generally three oxidation waves were observed between -0.2 V to 0.8 V for complexes **1-9**, see Figure 3. In the reduction region, depending on the NHC substituents, either one or two reduction processes were observed for complexes **1-9**. The non-NO_2-containing complexes each exhibited one irreversible reduction peak, while the NO_2-containing complexes exhibited one irreversible reduction process, followed by a chemically and electrochemically reversible reduction process.

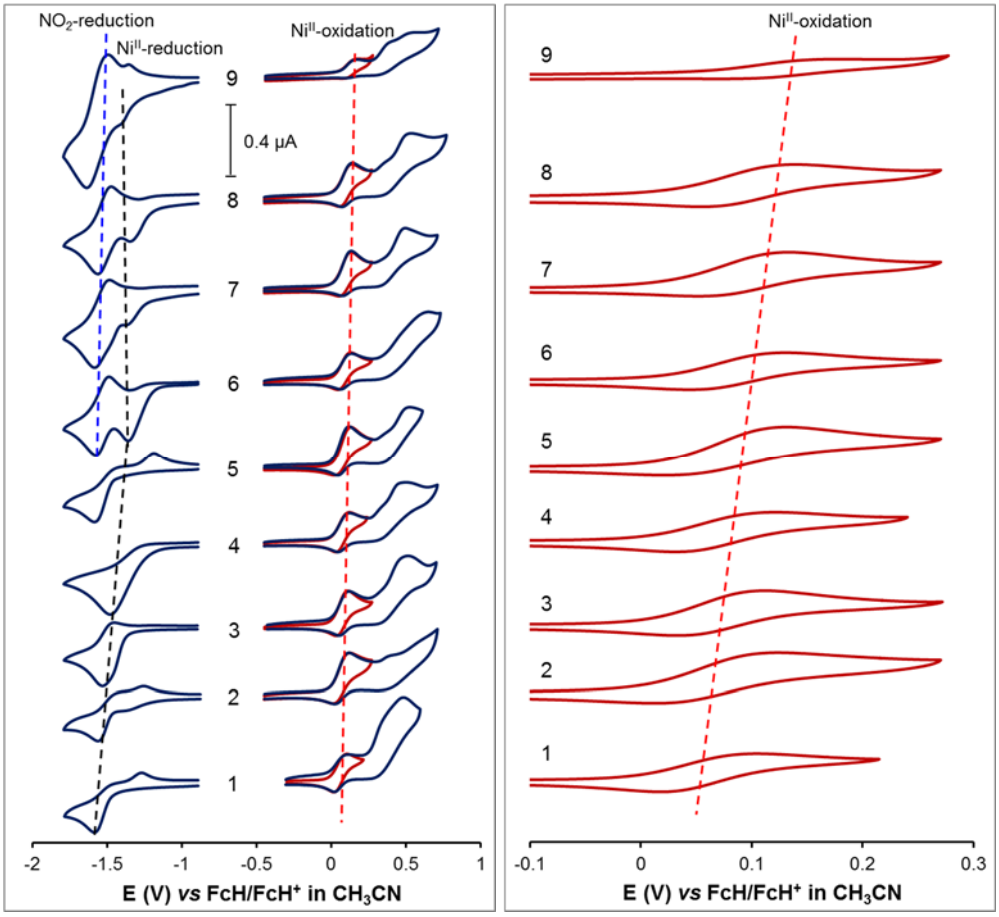

Figure 3: Comparative cyclic voltammograms (*vs.* FcH/FcH^+) at a scan rate of 0.1 $V.s^{-1}$ for complexes [CpNiBr(NHC)] **1-9**. Left: The reduction region between -1 V - -2 V *vs.* FcH/FcH^+, and the oxidation region -0.4 V – 1 V *vs.* FcH/FcH^+. Scans in red indicate the Ni^{II}/Ni^{III} redox couple. Right: Enlarged window of Ni^{II}/Ni^{III} redox couple shown for the oxidation region -0.1 V – 0.3 V *vs.* FcH/FcH^+. CVs were measured in 0.1 $mol.dm^{-3}$ $[NBu_4][PF_6]/CH_3CN$ on a glassy carbon working electrode at 25 °C. [Ni] = 0.002 $mol.dm^{-3}$ or saturated solution.

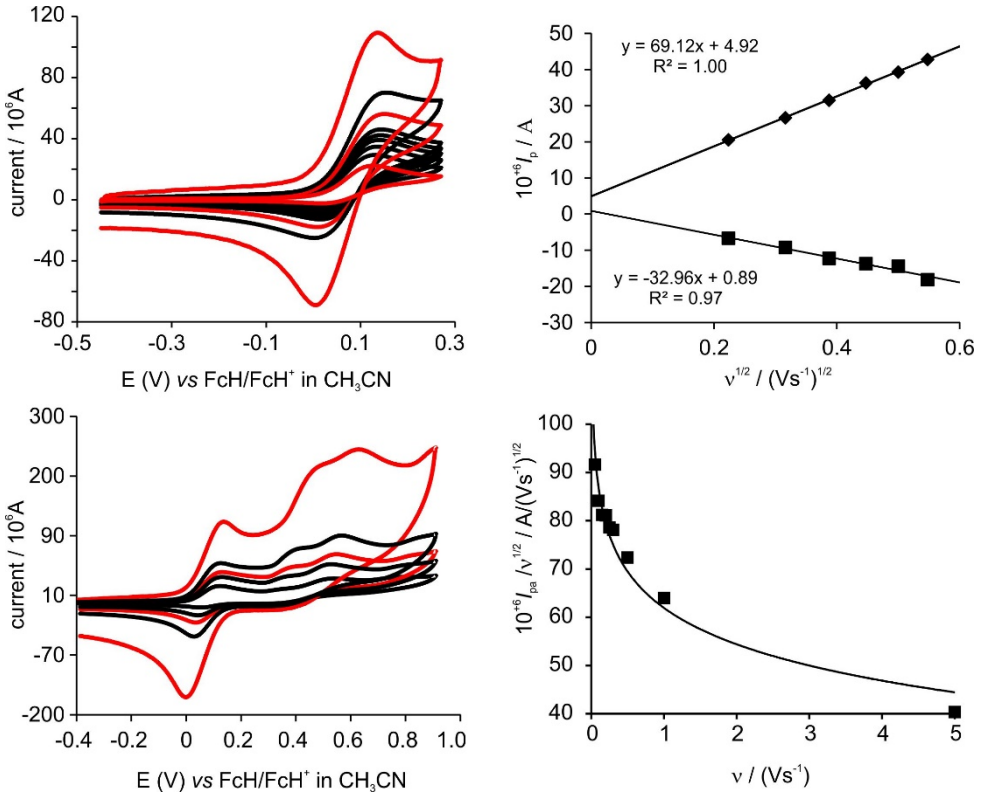

Figure 4: Top Left: Cyclic voltammograms of complex **5** at scan rates of 0.05 (red, lowest peak current), 0.10, 0.15, 0.20, 0.25, 0.30 0.50 (red), 1.00, 5.00 (red, highest peak current) $V.s^{-1}$. Bottom Left: Cyclic voltammograms of complex **5** at scan rates of 0.01 (lowest peak current), 0.30 0.50 (red), 1.00, 5.00 (red, highest peak current) $V.s^{-1}$. Scans were initiated in the positive direction. Top Right: The linear relationship between peak currents (i_p) and $(\text{scan rate})^{½}$ for the oxidation and reduction of complex **5**, is described by the Randles-Sevcik equation. Bottom Right: Dependence of $i_{pa}\nu^{-1/2}$ on scan rate ν.

3.3.1 Oxidation region

The first observed electrochemical process is an electrochemically reversible and chemically quasi-reversible oxidation process, with $0.062 \leq \Delta E_p \leq 0.127$ V, and $0.3 \leq i_{pc}/i_{pa} \leq 0.6$ at a scan rate $\nu = 0.1$ V s^{-1} (Figure 3). The average peak separation of the first oxidation process is slightly larger than the Nernstian value of 0.059 V for a one electron process due to uncompensated ohmic drops in the cell [42]. A graph of peak current *vs.* $\nu^{1/2}$ for the first oxidation peak revealed a linear relationship for scan rates in the regions 0.05 – 0.30 V s^{-1} (Figure 4 for **5**, data in Table 2 and Supplementary Information for **1-4** and **6-9**), indicating an essentially diffusion-controlled electrochemical process for **1-9**. The first oxidation-reduction wave becomes chemically more reversible at increased scan rates (Figure 4 left and

peak current ratio values in Table 2). The decrease of $i_{pa}\nu^{-1/2}$ *versus* increasing scan rate ν (see Figure 4 bottom right) indicates that reactions coupled to the initial electron transfer are present (EC mechanism) [43]. The first reversible oxidation peak is associated with the Ni^{II}/Ni^{III} redox couple. The second and third oxidation peaks are assigned to ligand oxidation (Figure 3). The assignment of the oxidation processes observed is supported by the findings of the DFT study of the frontier orbitals of complexes **1**-**9** presented in section 3.4. The assignment of the Ni^{II}/Ni^{III} redox couple is also in agreement with published results on related [CpNiX(NHC)] (X = Cl, I) complexes [25].

From Figure 3 it is clear that the formal reduction potential, $E^{\circ\prime}$, of the Ni^{II}/Ni^{III} redox couple for each of the complexes **1**-**9** is affected by the change of substituents on the coordinated NHC ligand, with $E^{\circ\prime}$ varying between 0.062 V and 0.127 V at ν = 0.100 V s^{-1}. Due to the range of *N*-substituents, the overall electron-donating (push) or electron-withdrawing (pull) properties of the NHC ligands differ. These substituents include Me, Bn (benzyl = C_7H_7), phenethyl, $(CH_2)_2Ph$, and 4-NO_2Bn. Of the NHC ligands, the Me substituted derivatives should be the most electron donating [44,45,46], while the 4-NO_2Bn substituted ligands will be the most electron withdrawing [41]. Substantial aromatic character exists in the *N*-heterocyclic ring due to the delocalisation of six π-electrons (sextet) within the ring [47,48,49]. Consequently, rapid electronic communication between the two *N*-substituents *via* the *N*-heterocyclic ring to the nickel centre is expected. The electron-donating or electron-withdrawing effect of the two *N*-substituents would thus be summative, resulting in the total electron-donating or electron-withdrawing (push-pull) effect for a specific NHC ligand. This push-pull effect may be quantified in terms of Hammett constants [50] associated with benzene-containing *N*-substituents (benzyl, phenethyl, 4-NO_2-benzyl). The *para*-substituent constant (σ_{para}) is considered; σ_{para} = 0 (benzyl, phenethyl) and σ_{para} = +0.778 (4-NO_2-benzyl) with respect to benzene. The corresponding cumulative effect may be considered to give resultant *para*-substituent constants (σ_{res}) for each ligand: σ_{res} = 0 (**L1**-**L5**), +0.778 (**L6**-**L8**), and +1.556 (**L9**). An increase in the sum of the Hammett constants of the *para*-substituents on the phenyl ring is related to the increase of the electron withdrawing ability of the substituents [51]. The linear increase in formal reduction potential, $E^{\circ\prime}$, of the Ni^{II}/Ni^{III} redox couple and the sum of the Hammett constants of the *para*-substituents (Figure S1 in the Electronic Supplementary Information) imply that good electronic communication between

the metal centre and different *para*-substituents on the phenyl ring of the *N*-substituents (benzyl, phenethyl, 4-NO_2-benzyl) exists.

The formal reduction potentials $E^{\circ\prime}$ of the Ni^{II}/Ni^{III} redox couple of complexes **4** and **5** are the same, indicating that the electron donating properties of Bn and $(CH_2)_2Ph$ are comparable. However, the $E^{\circ\prime}$ values of the non-NO_2-containing complexes **1**-**5**, all lie in a small range of 0.014 V (0.062-0.076 V), indicative of the similar electron donating properties of Me, Bn and the $(CH_2)_2Ph$ group. Complexes **1** and **2**, containing Me, Bn and $(CH_2)_2Ph$ groups, exhibited the lowest $E^{\circ\prime}$ potentials for all complexes **1**-**9**. The range of four NO_2-containing complexes **6**-**9**, is larger, namely 0.039 V (0.088-0.127 V). Introduction of a NO_2-group as a 4-NO_2Bn substituent on the NHC ligand, leads to an increase (more positive shift) of the formal reduction potential with *ca.* 0.01-0.02 V for the Ni^{II}/Ni^{III} redox couple (compare **6** with **1**, **7** with **5** or **8** with **4**). The synergy of the two 4-NO_2Bn substituents on the NHC ligand is clearly demonstrated when comparing **9** with **5**, where a 0.05 V increase (more than double the effect of one 4-NO_2Bn substituent alone) is observed. Complex **9**, with two 4-NO_2Bn substituents on the NHC ligand, exhibits the most positive (cathodic) potential (0.127 V) of complexes **1**-**9**.

The $E^{\circ\prime}$ values for the Ni^{II}/Ni^{III} wave obtained for **1**-**9** are in good agreement with those of Crabtree and co-workers [25]. For instance, they found $E_{1/2(ox)}$ = 0.033 V *vs.* FcH/FcH^+ for the complex [CpNiCl(IMes)]. This value, which is less positive (more negative) compared to the same redox couple for **1**-**9**, is expected when considering the electron donating mesityl substituents on the NHC ligand. Compared to the complex [CpNiCl(IMes)], complexes **1**-**9** all contain less electron-donating NHC ligands. The Ni^{II}/Ni^{III} redox potential is more negative ($E_{1/2(ox)}$ = -0.130 V) for the complex [CpNiI(IMe)] (IMe = 1,3-dimethylimidazol-2-ylidene), where the electron-withdrawing chlorido ligand (Pauling electronegativity 3.16) was exchanged for the far less electron-withdrawing iodo ligand (Pauling electronegativity 2.66). Conversely, they found noticeably higher (more positive) $E_{1/2(ox)}$ values when electron-withdrawing functionalities were incorporated on the imidazolyl backbone of the NHC ligand, e.g. $E_{1/2(ox)}$ = 0.073 V (with two Cl-substituents, [CpNiI($IMeCl_2$)]) ($IMeCl_2$ = 4,5-dichloro-1,3-dimethylimidazol-2-ylidene), and $E_{1/2(ox)}$ = 0.124 V (with two CN-substituents, [CpNiI(IMe{CN}$_2$)]) (IMe{CN}$_2$ = 4,5-dicyano-1,3-dimethylimidazol-2-ylidene). This indicates that substituent variations on the imidazolyl backbone may noticeably affect metal-

centred redox processes, apart from the effect of different *N*-alkyl/aryl substituents on NHCs itself.

Table 1: Electrochemical data (*vs.* FcH/FcH^+) for redox processes observed for **1-9**.

Complex	R^b	R'^b	Ni^{II}/Ni^{III} (V)					2nd oxidation (V)	3rd oxidation (V)	1st reduction (V)	2nd reduction (V)	Re-oxidation[e]
			E_{pa}	E_{pc}	ΔE_p	$E^{\circ\prime}$	I_{pc}/I_{pa}	E_{pa}	E_{pa}	E_{pc}	E_{pc}	E_{pa}
1	Me	Bn	0.106	0.018	0.088	0.062	0.6	0.336	0.482	-1.498	-	-
2	$(CH_2)_2Ph$	$(CH_2)_2Ph$	0.124	0.013	0.111	0.068	0.4	0.36[c]	0.575	-1.546	-	
3	Me	$(CH_2)_2Ph$	0.112	0.032	0.080	0.072	0.4	0.33[c]	0.515	-1.531	-	-
4	Bn	$(CH_2)_2Ph$	0.122	0.031	0.091	0.076	0.5	0.340	0.501	-1.480	-	-
5	Bn	Bn	0.132	0.021	0.111	0.076	0.4	0.336	0.538	-1.585	-	-
6	Me	$4\text{-}NO_2Bn$	0.132	0.045	0.087	0.088	0.5	0.49[c]	0.652	-1.360	-1.574	-1.490
7	Bn	$4\text{-}NO_2Bn$	0.134	0.052	0.082	0.093	0.3	0.36[c]	0.495	-1.378	-1.584	-1.484
8	$(CH_2)_2Ph$	$4\text{-}NO_2Bn$	0.140	0.054	0.086	0.097	0.4	0.368	0.534	-1.347	-1.563	-1.474
9	$4\text{-}NO_2Bn$	$4\text{-}NO_2Bn$	0.181	0.073	0.108	0.127	0.4	0.396	0.559	-1.388	-1.553, -1.657	-1.493, -1.355
Nc[a]	-	-	-0.468	-0.356	0.112	-0.412	1.0	0.507[d]	-	-2.169	-	-

[a] Nc = nickelocene, $NiCp_2$. [b] Bn = benzyl; $(CH_2)_2Ph$ = phenethyl; $4\text{-}NO_2Bn$ = $4\text{-}NO_2$-benzyl. [c] Cannot determine accurately, 2nd and 3rd oxidation peaks are overlapping. [d] $E^{\circ\prime}$ (V). [e] Oxidation of NO_2 group attached to di-anion.

Table 2: Electrochemical data (*vs.* FcH/FcH^+) in CH_3CN for *ca*. 0.002 mol dm^{-3} of complex **5** at indicated scan rates.

ν ($V.s^{-1}$)	E_{pa} (V)	E_{pc} (V)	ΔE (V)	$E°'$ (V)	$10^6 I_{pa}$ (A)	$10^6 I_{pc}$ (A)	I_{pc}/I_{pa}
0.05	0.015	0.127	0.112	0.071	20.5	6.7	0.33
0.10	0.021	0.132	0.111	0.076	26.6	9.3	0.35
0.15	0.020	0.137	0.117	0.078	31.5	12.3	0.39
0.20	0.018	0.139	0.121	0.078	36.3	13.7	0.38
0.25	0.017	0.143	0.126	0.080	39.3	14.4	0.37
0.30	0.015	0.145	0.130	0.080	42.8	18.1	0.42
0.50	0.009	0.150	0.141	0.079	51.2	23.5	0.46
1.00	0.003	0.155	0.152	0.079	64.0	29.2	0.46
5.00	0.006	0.138	0.132	0.072	89.7	58.1	0.65

Following the first oxidation process (Ni^{II}/Ni^{III}), two distinct irreversible oxidation waves are observed for all complexes. The second oxidation process lies at $E_{pa} \approx 0.37$ V (Figure 3) and the third oxidation process at $E_{pa} \approx 0.5$ V. The second oxidation process was assigned as an irreversible halide oxidation by Crabtree *et al.* [25], although they mentioned that ligand participation could not be excluded. They also observed irreversible oxidation waves between $0.218 \text{ V} \leq E°' \leq 0.282$ V for their CpNi(NHC) halide complexes, following the Ni^{II}/Ni^{III} redox couple. After close inspection from DFT studies (see section 3.4) the second and third oxidation processes of complexes **1**-**9** of this study were concluded to be NHC ligand based, and not bromide-based, processes. For the second oxidation process a similar trend as for the Ni^{II}/Ni^{III} oxidation process is observed, where the electron-donating NHCs exhibit less positive (more negative) potentials, compared to the more electron-withdrawing NO_2-containing NHCs **6**-**9**, which have more positive potentials.

3.3.2 Reduction region

Depending on the NHC substituents, either one or two reduction processes were observed for complexes **1**-**9**. The non-NO_2-containing complexes **1**-**5** each exhibited one irreversible reduction peak ($-1.480 \text{ V} \leq E°' \leq -1.585$ V) assigned to Ni^{II}/Ni^{I} reduction. This is based on the character of the LUMO of these complexes determined by the DFT study in section 3.4. Crabtree *et al.* [25] also interpreted a quasi-reversible reduction wave at -1.510 V *vs.* FcH/FcH^+ of the complex [CpNiCl(IMes)] as Ni^{II}/Ni^{I} reduction. The small re-oxidation peaks observed for **1** (*ca*. -1.25 V), **2** (*ca*. -1.23 V) and **5** (*ca*. -1.15 V) are ascribed to the

oxidation of the unknown product of the Ni^{II}/Ni^{I} reduction, since no re-oxidation peaks were observed when the CVs were turned around at -1.35 V.

The four 4-NO_2Bn-containing NHC complexes **6**-**9**, each show at least two reduction peaks and one re-oxidation peak. The two or more reductions observed are related to the two redox active centres (NO_2 and Ni(II)) for **6**-**8** and the three redox active centres for **9**. No re-oxidation peak or reversibility is observed when the scan was reversed just after the first reduction peak. The order of reduction of these complexes can be interpreted in one of the following ways:

(i) First peak is assigned to Ni^{II}/Ni^{I} reduction: It is expected that Ni(II) in complexes **6**-**9** will be reduced at a higher (less negative potential) than the non-4-NO_2Bn-containing complexes **1**-**5**, due to the electron withdrawing properties of the NO_2 moiety. This explains why the first reduction peak of **9** is *ca*. 0.2 V more positive (less negative) than that of **5**, with a similar trend when comparing **7** with **5** and **8** with **4** or **6** with **1**. The first and second reduction peaks for **6**-**9** are observed at -1.35 to -1.39 V and -1.55 to -1.58 V, respectively (*ca*. 0.2 V apart). Reversible NO_2 (nitro-benzene) reduction is expected at *ca.* -1.5 V [41], for example *para*-NO_2-toluene (a comparable derivative) was observed at $E^{0\prime}$ (Fc/Fc^{+}) = -1.547 V when obtained under the same experimental conditions [41]. This leads to the interpretation that the first reduction peak observed for complexes **6**-**9** is the Ni^{II}/Ni^{I} reduction, followed by the second reversible couple assigned to NO_2 reduction. For complex **9,** the first reduction peak is followed by a larger second reduction peak, nearly double the peak current of that of the first reduction process. Two re-oxidation peaks are obtained for **9**, see Figure 5. The large double peak current reduction peak and the two re-oxidation peaks are consistent with the near simultaneous reduction of the two NO_2 groups after the initial Ni^{II}/Ni^{I} reduction. The reduction of the two NO_2 groups directly after the Ni^{II}/Ni^{I} reduction of **9** was much better resolved by Osteryoung square wave voltammetry, see Figure 5.

(ii) First peak is assigned to NO_2 reduction with rapid charge transfer to Ni^{II}: When evaluating the character of the LUMOs of complexes **6**-**9** (section 3.4.2 below), the LUMO is located on the NO_2-moiety of the 4-NO_2Bn substituent. From a DFT point of view, the first reduction of complexes **6**-**9** is thus NO_2 reduction. Then the electron added upon the first reduction undergoes rapid intramolecular charge transfer from the NO_2 group to involve Ni^{II}/Ni^{I} reduction, followed by NO_2 reduction (the second reduction peak). This will explain why the re-oxidation peak of the NO_2 moiety is negative compared to the first reduction peak for **6**-**8**.

(iii) First peak is assigned to NO_2 reduction followed by Ni^{II}/Ni^{I} reduction: Since the LUMOs of complexes **6-9** (section 3.4.2 below) are located on the NO_2-moiety of the 4-NO_2Bn substituent, the first NO_2 reduction is followed by Ni^{II}/Ni^{I} reduction of NO_2-reduced species of **6-9** (the second reduction peak), forming a di-cationic species. To explain why the re-oxidation peak of **6-8** is negative of the first NO_2-reduction peak, charge transfer may occur from Ni^{I} to the NO_2^- moiety, making re-oxidation of the NO_2 group easier (associated with a Ni^{I} complex) at a lower potential than the reduction of the NO_2 group associated with a Ni^{II} complex. The fact that no re-oxidation peak is observed when the scan was reversed just after the first reduction peak of **6-9** excludes (iii) here.

Thus from an experimental point of view, the first reduction involves Ni^{II}/Ni^{I} reduction, either directly as proposed in (i) above, or indirectly as proposed in (ii) above. The DFT results below favour (ii), namely that the electron added upon the first reduction involving NO_2, undergoes rapid intramolecular charge transfer from the NO_2 group to involve Ni^{II}/Ni^{I} reduction, followed by NO_2 reduction (the second reduction peak).

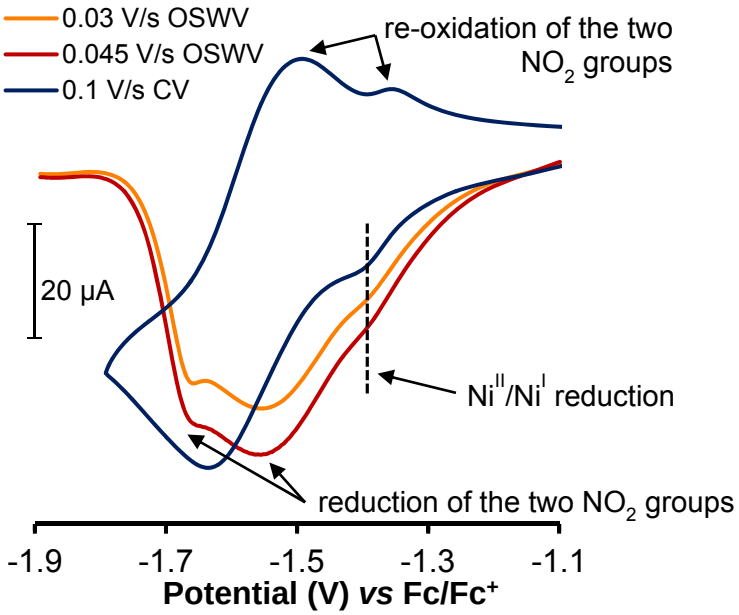

Figure 5: Cyclic voltammogram (CV, scan rate = 0.100 $V.s^{-1}$) and Osteryoung square-wave voltammograms (OSWV, scan rate of 0.03 and 0.045 $V.s^{-1}$) showing the reduction region of **9**.

Linear sweep voltammograms (LSVs), obtained at a stationary electrode at a slow scan rate for the oxidation and the reduction of **1, 8** and **9** are shown in Figure 6, as an example of the amount of electron(s) involved in the different electrochemical processes for non-4-NO_2-benzyl substituted NHCs (**1**-**5**), the mono-4-NO_2-benzyl substituted NHCs (**6**-**8**) and the bis-4-NO_2-benzyl substituted NHC complex (**9**).

(i) a one-electron oxidation : one-electron reduction process for **1**-**5**,

(ii) a one-electron oxidation : one-electron first reduction process : one-electron second reduction process for **6**-**8**, and

(iii) a one-electron oxidation : one-electron first reduction process : near simultaneous reduction of the two electrons second reduction process for **9**.

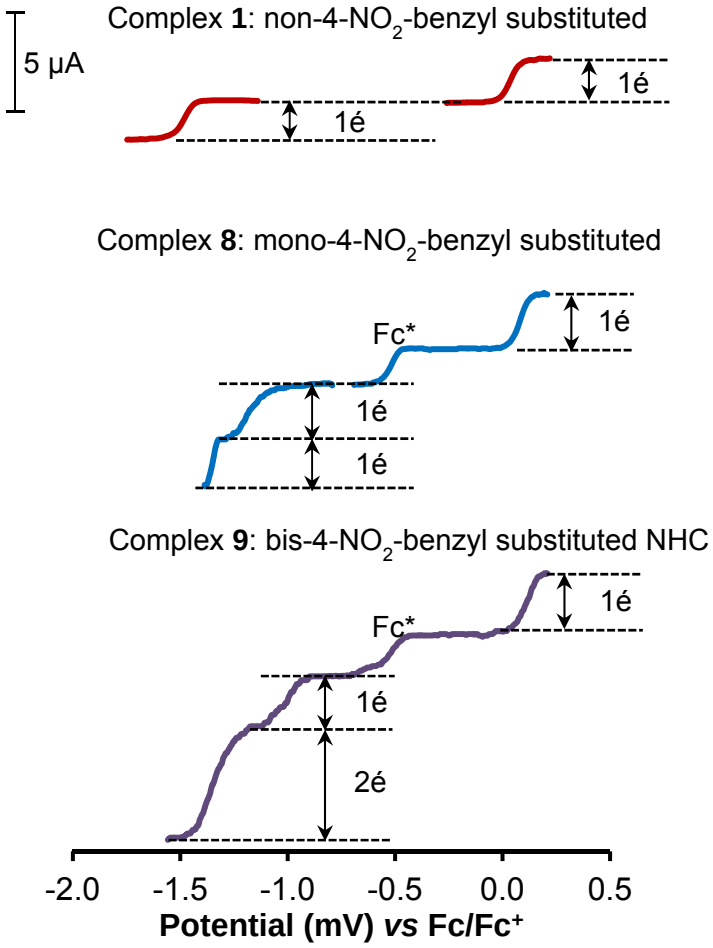

Figure 6: The linear sweep voltammograms (LSVs) of **1**, **8** and **9** at a scan rate of 0.002 $V.s^{-1}$. Decamethyl ferrocene (Fc*, -0.508 V *vs.* FcH/FcH^+) was used as internal standard.

For further confirmation of the assignment of the observed redox processes for **1-9**, the cyclic voltammogram of nickelocene was obtained under the same experimental conditions, with data reported in Table 1. The redox values obtained for nickelocene in this study are in agreement with published data obtained under similar experimental conditions [52,53]. The two oxidation processes are assigned to the reversible Ni^{II}/Ni^{III} oxidation at -0.468 V, followed by the reversible Ni^{III}/Ni^{IV} oxidation nearly 1 V higher at 0.507 V. One irreversible reduction process (Ni^{II}/Ni^{I}) is observed at -2.169 V, *ca.* 1.7 V more negative than the Ni^{II}/Ni^{III} oxidation. The difference between the Ni^{II}/Ni^{III} oxidation and the Ni^{II}/Ni^{I} reduction for the non-NO_2-containing complexes **1-5** is 1.6-1.7 V, similar to the difference obtained for nickelocene. However, the difference between the Ni^{II}/Ni^{III} oxidation and the second and the third oxidation processes for **1-9** is *ca.* 0.2 V and 0.4 V, respectively. Analogous to nickelocene, the second and third oxidation processes for **1-9** are therefore far too low to be metal-based, and thus in agreement with the NHC ligand based assignment for the second and third oxidation processes.

3.4 DFT studies

In order to better understand the oxidation and reduction processes observed, a density functional theory (DFT) study of complexes **1-9** is presented. Different orientations for the benzyl (Bn), phenethyl ($(CH_2)_2Ph$), and 4-nitrobenzyl (4-NO_2Bn) *N*-substituents for each of the complexes **1-9** were evaluated, in order to find the conformation of global minimum energy. It is possible for the phenyl ring of the benzyl, phenethyl, or 4-nitrobenzyl *N*-substituents to be orientated 'above' (A) or 'below' (B) the imidazolylidene ligand plane, see Figure 7 for complex **5** as an example. For all complexes **1-9**, conformation BB with both *N*-substituents situated below the plane of the imidazolylidene ligand was the lowest in energy.

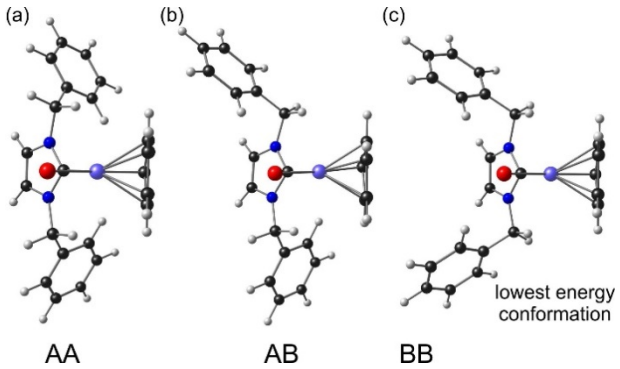

Figure 7: The three different *N*-substituent orientations possible for **5**. Colour code used for atoms: Ni (violet), N (dark blue), Br (red), C (grey), and H (white).

Table 3: Relative energies (eV) of the optimised isomers of complexes **1**-**9**.

Complex	*E* (eV)	Isomer[a]	X-ray structure reference
1	0.00	B	[30]
	0.05	A	
2	0.00	BB	
	0.07	AB	[31]
	0.15	AA	
3	0.00	B	
	0.07	A	[30]
4	0.00	BB	
	0.05	BA	
	0.07	AB	
	0.13	AA	
5	0.00	BB	
	0.04	AB	
	0.10	AA	[30]
6	0.00	B	[30]
	0.08	A	
7	0.00	BB	
	0.06	BA	
	0.04	AB	[31]
	0.12	AA	
8	0.00	BB	
	0.07	BA	
	0.07	AB	
	0.14	AA	[31]
9	0.00	BB	
	0.05	AB	
	0.14	AA	

[a] The terms above (A) and below (B) refer to the relative conformation of the relevant *N*-substituent with respect to the imidazolylidene ring.

This implies that the conformer with the phenyl ring(s) of either the benzyl, phenethyl, or 4-nitrobenzyl *N*-substituents directed away from the Cp ring (Figure 7(c), conformer BB), minimised the energy of the resultant complex, while conformation AA was found to have the highest energy (Table 3). The conformations of the lowest energy gas phase calculated isomers did not always correspond to solid state X-ray structures, where intrinsic forces such as π-π stacking between phenyl rings and other stabilisation interactions may lead to a lower energy isomer as the one calculated.

3.4.1 Non-NO_2-containing Ni(II)-NHCs

To understand the electrochemical origin of the first oxidation and first reduction processes observed for the non-NO_2-containing complexes **1**-**5**, selected frontier molecular orbitals (MOs) of complex **5** are shown in Figure 8 as a representative example. Since oxidation involves removal of an electron from the HOMO of the neutral complex, the HOMO of the neutral complex or the LUMO of the oxidised species (MO where the electron was removed), suggests the origin of the first oxidation process. The Mulliken spin density plot of the oxidised complex indicates the locus of the remaining unpaired electron of the cation. The HOMO of neutral **5** has 32% Ni d_π, 17% Br and 34% Cp character, the LUMO of oxidised **5** has 55% Ni d_π, 11% Br and 22% Cp character, while the spin density plot of oxidised **5** has 72% Ni d_π, 8% Br and *ca.* 25% Cp character (Table 4). The first oxidation process of complexes **1**-**5** is thus mainly Ni-metal based, involving the Ni^{II}/Ni^{III} redox couple with a minor amount of radical character on the Cp ring [54]. The oxidation processes following the Ni^{II}/Ni^{III} redox couple are proposed to be centred on the phenyl substituent of the NHC ligand. This conclusion was drawn based on the character of the near degenerate HOMO (α-HOMO) and HOMO-1 (β-HOMO) of oxidised **5**, *i.e.* $[\mathbf{5}]^+$ ($\mathbf{5} - 1e^-$), both of similar NHC ligand character (Figure 8(c)).

Similarly, the LUMO of the neutral species (Figure 8a), 45% Ni-$d_{x^2-y^2}$ suggests metal-centred reduction (Ni^{II}/Ni^{I}), for **5**. Since molecular orbitals often re-arrange after reduction [55], the inspection of the characters of the HOMOs and spin density profile of the reduced compound becomes important. The spin density of the reduced compound shows the distribution of the added unpaired electron. For the reduced species of **5**, the HOMO (β-HOMO of d_π + Cp character) is *ca.* 0.25 eV higher than the HOMO-1 (α-HOMO of $d_{x^2-y^2}$ + Cp character), with both exhibiting Ni-d character. The spin density profile of 86% Ni and 5% Br character indicates that the nature of the electron added upon reduction is mainly Ni-d-based, thereby confirming the first observed reduction process for **5** to be Ni^{II}/Ni^{I} reduction. Similarly, the anions of **1**-**5** all have 86-90% Mulliken spin density of Ni-d character, whereas the cations of **1**-**5** all have *ca.* 72% Mulliken spin density of Ni-d_π character (Table 4). The DFT results thus clearly indicate that the first oxidation and the first reduction processes observed for the Ni(II)-NHC complexes **1**-**5**, involve Ni^{II}/Ni^{III} oxidation and Ni^{II}/Ni^{I} reduction respectively.

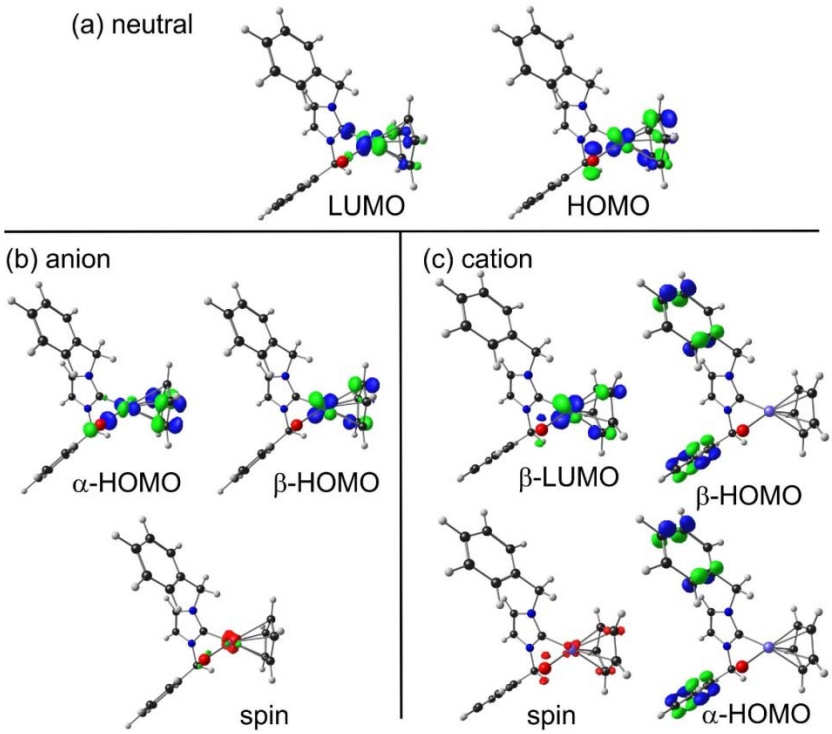

Figure 8: Selected molecular orbitals (green and blue) and Mulliken spin plots (red) of **5**: (a) neutral, (b) reduced (1e$^-$ addition) and (c) oxidised (1e$^-$ removal). Colour code used for atoms: Ni (violet), N (dark blue), Br (red), C (grey) and H (white).

3.4.2 NO_2-containing Ni(II)-NHCs

The HOMO of the neutral complex, the LUMO of oxidised species (removed electron) as well as the Mulliken spin density plot of the oxidised complex of the NO_2-containing Ni(II)-NHC complexes **6**-**9** provide insight in the origin of the first oxidation process of complexes **6**-**9** (complex **6** as representative example, Figure 9). A comparison of Figure 8(a, c) with Figure 9(a, c), as well as the data in Table 4 reveals a similar character of the HOMO of **6**-**9** to that of the non-NO_2-containing Ni(II)-NHC complexes **1**-**5**. The first oxidation process of complexes **6**-**9** is mainly Ni-metal based, involving the Ni^{II}/Ni^{III} redox couple. However, the oxidations following the Ni^{II}/Ni^{III} redox couple of **6**-**9** are proposed to be centred on the NO_2-group of the NHC ligand. This proposal is based on the character of the near degenerate HOMO (α-HOMO) and HOMO-1 (β-HOMO) of oxidised **6**, *i.e.* $[\mathbf{6}]^+$ (**6** – 1e$^-$), with both of mainly NO_2 character (Figure 9(c)).

The LUMO and LUMO+1 of **6** are NO_2 and Ni-based respectively, suggesting the first reduction of **6** is NO_2-based. However, the HOMO (β-spin) of reduced **6** has 49% Ni character with some NO_2 contribution, suggesting a non-innocent NO_2-moiety. It is believed that the electron added upon reduction undergoes rapid intramolecular charge transfer from the NO_2 group to involve Ni^{II}/Ni^{I} reduction. The reduced complex is a Ni(I) complex, since the spin density of reduced **6** is 96% Ni, with a spin density profile similar to that of the non-NO_2-containing Ni(II)-NHC complexes **1**-**5**; compare Figure 8(b) with Figure 9(b), as well as the data in Table 4.

The LUMO (β-spin) of reduced **6** has 51% NO_2 character with only 13% Ni character, strongly suggesting that the second reversible reduction observed involves NO_2 (Figure 9). This interpretation also applies to the reduction of complexes **7** and **8**, (Table 4), and is in agreement with the experimental observation that the first reduction for complexes **6**-**8** involves the Ni^{II}/Ni^{I} couple, followed by the second reversible couple assigned to NO_2 reduction. With virtually no spin density on Ni for the anion of complex **9**, the interpretation follows that charge transfer took place after Ni reduction of **9** to the two electron withdrawing NO_2 groups, before reduction of the two NO_2 groups occurs.

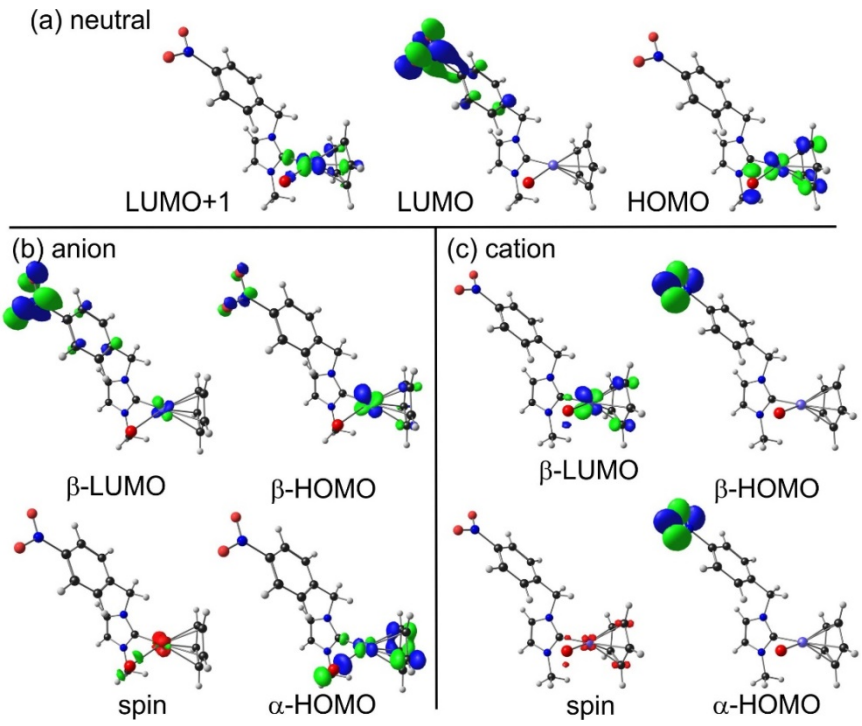

Figure 9: Selected molecular orbitals (green and blue) and Mulliken spin plots (red) of **6**: (a) neutral, (b) reduced ($1e^-$ addition) and (c) oxidised ($1e^-$ removal). Colour code used for atoms: Ni (violet), N (dark blue), O (red), Br (red), C (grey) and H (white).

Table 4: DFT calculated energies (eV) of the neutral and atomic Mulliken spin density of reduced (anion) and oxidised (cation) of **1-9**.

	Neutral			Cation				Anion						
	E_{HOMO}	E_{LUMO}	IP	Ni	Br	C_{NHC}	Cp ring total	Ni	Br	N	O	O	C_{NHC}	Cp ring total
1	-5.071	-1.707	6.304	0.719	0.079	-0.031	0.013	0.884	0.047	-	-	-	0.025	0.053
2	-5.114	-1.761	6.281	0.721	0.076	-0.030	-0.092	0.860	0.045	-	-	-	0.030	0.042
3	-5.065	-1.713	6.300	0.719	0.079	-0.030	-0.091	0.901	0.045	-	-	-	0.020	0.011
4	-5.126	-1.768	6.284	0.723	0.076	-0.031	-0.091	0.875	0.046	-	-	-	0.025	0.012
5	-5.107	-1.742	6.273	0.724	0.075	-0.032	-0.002	0.863	0.047	-	-	-	0.030	0.076
6	-5.305	-2.657	6.536	0.719	0.078	-0.029	-0.005	0.956	0.061	-0.050	-0.041	-0.037	0.040	0.041
7	-5.336	-2.650	6.496	0.722	0.076	-0.030	-0.002	0.934	0.057	-0.037	-0.031	-0.033	0.037	0.058
8	-5.347	-2.673	6.502	0.721	0.076	-0.029	-0.093	0.920	0.055	-0.030	-0.029	-0.026	0.035	0.006
9	-5.556	-2.794	6.703	0.720	0.076	-0.029	-0.093	0.000	0.000	0.096	0.089	0.094	0.002	0.000

3.4.3 Catalytic activities, redox potentials and DFT energies

A simple plot of molecular orbital energies of complexes **1-9** clearly illustrated the effect of the electron-withdrawing 4-NO_2-benzyl substituent (Figure 10): A slight lowering of HOMO energies, combined with noticeable lowering of LUMO energies resulted in smaller HOMO-LUMO energy gaps, which necessarily indicate less stable and more reactive species for **6-9** [56]. This was also confirmed in catalytic studies involving complexes **1-9**, where the 4-NO_2Bn-containing Ni-NHC complexes exhibited the lowest substrate conversions along with the lowest TOFs in the Suzuki-Miyaura coupling of 4-chlorophenyl carboxaldehyde with phenylboronic acid [30], as well as in the anaerobic oxidation of secondary alcohols [31]. In these catalytic studies, the more electron-donating Ni-NHC complexes were the most efficient, because they were the least susceptible to catalyst deactivation/decomposition throughout the course of the reactions [31].

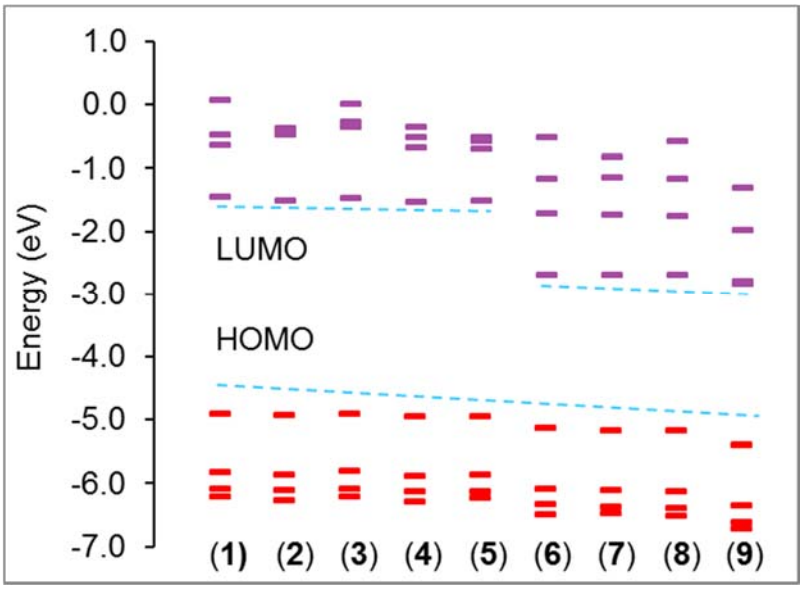

Figure 10: Molecular orbital energy levels (eV) of **1-9**. (1 eV = 96.485 kJ.mol^{-1})

The graph of the formal reduction potential, $E^{o'}$ (V), of the Ni^{II}/Ni^{III} couple, as a function of the C-C coupling product yield (%) from the Suzuki-Miyaura reaction [30], is shown in Figure 11(a). A trend between these two parameters is observed, as might be expected: The Suzuki-Miyaura mechanism relies on the capability of the Ni(II) catalyst to be constantly oxidised and reduced in solution, the ease of which could be probed using cyclic voltammetry. The more donating the bound NHC ligand, the higher electron density resides on the metal. Therefore, oxidation should occur faster and be more facile than those bearing

electron-withdrawing NHC ligands. Electron-donating NHCs render the Ni^{II}/Ni^{III} redox couple more negative (easier to oxidise at a lower potential), and hence lead to more efficient catalysts. The graph of the formal reduction potential, $E^{o'}$ (V), of the Ni^{II}/Ni^{III} couple, as a function of the % conversion when used as pre-catalysts in the chemoselective anaerobic oxidation of secondary aryl alcohols, shows a similar trend, Figure 11(b).

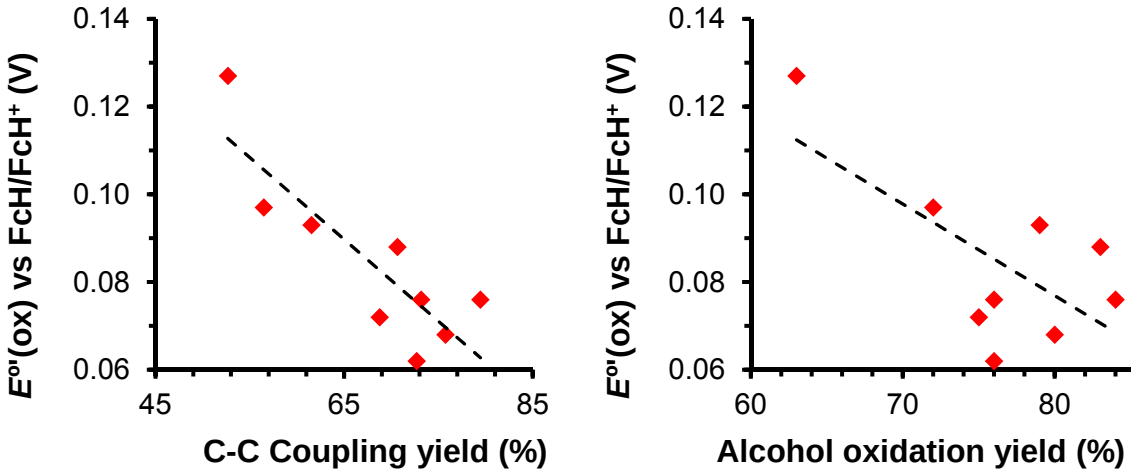

(a) (b)

Figure 11: Relationship between the formal reduction potential, $E^{0'}$ (V), of the Ni^{II}/Ni^{III} couple, as a function of (a) the C-C coupling product yield (%) from the Suzuki-Miyaura reaction and (b) % conversion when used as pre-catalysts in the chemoselective anaerobic oxidation of secondary aryl alcohols.

Electro-oxidation of a metal complex involves removal of electron(s) from the HOMO of the neutral complex, whereas electro-reduction involves the addition of electron(s) to the LUMO of the neutral complex. Therefore a relationship between the energy of the HOMO (E_{HOMO}), and $E^{o'}$ (Ni^{II}/Ni^{III}) exists. From Figure 12 these linear relationships are evident with relatively good correlation coefficients, and are in good agreement with the DFT-Koopmans' theorem that states that the first (vertical) ionisation energy of a system is related to the negative of the corresponding E_{HOMO} [57,58]. The DFT calculated energy needed to remove one electron from the HOMO of the neutral complex ($IP_{1é}$), *i.e.* the one-electron adiabatic ionisation potential, is also linearly related to $E^{o'}$ of the 1-electron redox couple (Ni^{II}/Ni^{III}). Hence, it is clear that the electron-withdrawing 4-NO_2Bn-containing NHC complexes require more energy for oxidation (more positive E_{pa} for Ni^{II}/Ni^{III}, more negative ionisation potential), as compared to the non-4-NO_2Bn-containing NHC complexes. This shows once more how

electron-donating *N*-substituents on NHC ligands evidently better stabilise the metal species, which may allow for the observation of higher oxidation state metal species [59].

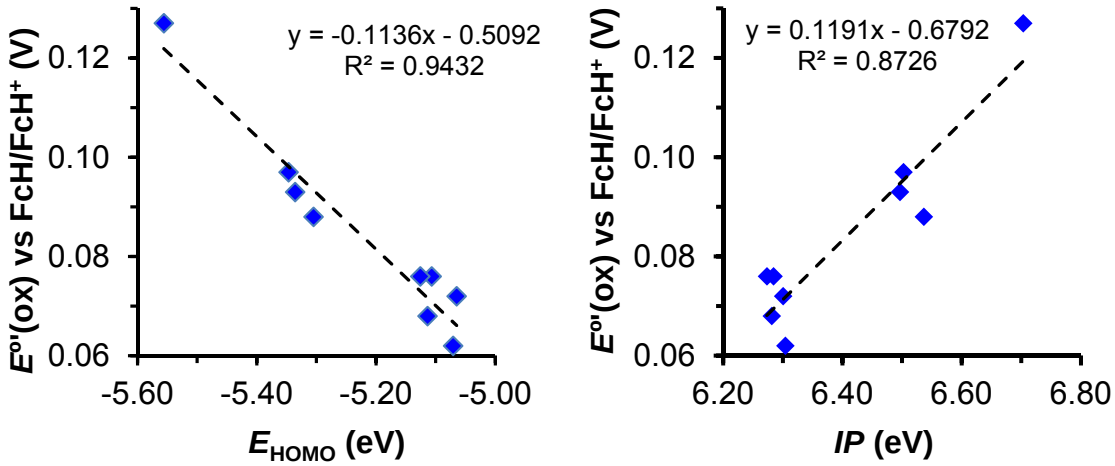

Figure 12: Graphs of electrochemical formal reduction potential, $E°'$, of the Ni^{II}/Ni^{III} couple, and the DFT calculated (a) E_{HOMO} and (b) IP_{1e}-, energies of **1**-**9**. Dotted lines indicate trend lines with the given formulae and correlation coefficients.

To test the applicability of the relationship $E°'$ (Ni^{II}/Ni^{III}) = -0.1136(E_{HOMO}) – 0.5092 (Figure 12 left), we optimised [CpNiCl(IMes)] that was reported to have a reversible $E°'$ (Ni^{II}/Ni^{III}) at 0.723 V *vs* NHE = 0.033 V vs FcH/FcH^+ [25]. The calculated E_{HOMO} of the DFT optimised [CpNiCl(IMes)] is -4.727 eV, giving a $E°'$ (Ni^{II}/Ni^{III}) value of 0.028 V that is within 0.005 V of the experimental value.

4. Conclusion

The range of flexible, electron-withdrawing and -donating NHC-containing [CpNiBr(NHC)] complexes were synthesised, and their electrochemical properties investigated by means of cyclic voltammetry, Osteryoung square wave voltammetry, linear sweep voltammetry and DFT methods. From the CVs several redox active oxidation waves and couples were observed and systematically concluded to be the quasi-reversible Ni^{II}/Ni^{III} redox couple followed by irreversible ligand-centred oxidations. During reduction, the irreversible Ni^{II}/Ni^{I} reduction wave was observed first for complexes **1**-**9**. A second reduction process, observed only for the NO_2-containing complexes **6**-**9**, involves NO_2-reduction. DFT studies supported these findings by providing further insight into the electrochemical nature of the specific

electrochemical processes observed for each of the complexes **1**-**9**. Electrochemically and computationally, the push-pull effect of the electron-donating *vs.* electron-withdrawing NHC ligands was evident and largely determines the ease of oxidation of Ni^{II} and related electrochemical events observed for complexes **1**-**9**.

Supplementary Information

Optimised coordinates of the DFT calculations and electrochemical graphs and data are given in the Supporting Information.

Acknowledgements

This work has received support from the South African National Research Foundation (JC Grant nr. 96111, ML Grant nr. 95764, FPM Grant nr. 88594) and the Central Research Fund of the University of the Free State, Bloemfontein (JC) and the University of Pretoria (ML). The High Performance Computing facility of the UFS and the Norwegian Supercomputing Program (NOTUR Grant nr. NN4654K) (JC) are acknowledged for computer time.

References

[1] L. M. Dornan, G. M. A. Clendenning, M. B. Pitak, S. J. Coles, M. J. Muldoon, *Catal. Sci. Technol.*, 2014, **4**, 2526-2534.
[2] J. A. Mueller, C. P. Goller, M. S. Sigman, *J. Am. Chem. Soc.*, 2004, **126**, 9724-9734.
[3] R. H. Crabtree, *Chem. Rev.*, 2015, **115**, 127-150.
[4] K. M. Gligorich, M. S. Sigman, *Angew. Chem. Int. Ed.*, 2006, **45**, 6612-6615.
[5] L. P. Bheeter, M. Henrion, L. Brelot, C. Darcel, M. J. Chetcuti, J-B. Sortais, V. Ritleng, *Adv. Synth. Catal.*, 2012, **354**, 2619-2624.
[6] R. H. Crabtree, *Coord. Chem. Rev.*, 2013, **257**, 755-766.
[7] O. Kühl, *Chem. Soc. Rev.*, 2007, **36**, 592-607.
[8] A. P. Prakasham, P. Ghosh, *Inorg. Chim. Acta.*, 2015, **431**, 61-100.
[9] R. Visbal, A. Laguna, M. C. Gimeno, *Chem. Comm.*, 2013, **49**, 5642-5644.
[10] O. Schuster, L. Yang, H. G. Raubenheimer, M. Albrecht, *Chem. Rev.*, 2009, **109**, 3445-3478.
[11] B. Landers, O. Navarro, *Inorg. Chim. Acta.*, 2012, **380**, 350-353.
[12] B. Landers, O. Navarro, *Eur. J. Inorg. Chem.*, 2012, 2980-2982.
[13] L-Y. Wang, J. Li, Y. Lv, H-Y. Zhang, S. Gao, *J. Organomet. Chem.*, 2011, **696**, 3257-3263.
[14] V. Ritleng, M. Henrion, M. J. Chetcuti, *ACS Catal.*, 2016, **6**, 890-906.
[15] C. D. Abernethy, A. H. Cowley, R. A. Jones, *J. Organomet. Chem.*, 2000, **596**, 3-5.
[16] W. Buchowicz, Ł. Banach, J. Conder, P. A. Guńka, D. Kubicki, P. Buchalski, *Dalton Trans.*, 2014, **43**, 5847-5857.
[17] A. M. Oertel, V. Ritleng, M. J. Chetcuti, *Organometallics*, 2012, **31**, 2829-2840.
[18] V. Ritleng, A. M. Oertel, M. J. Chetcuti, *Dalton Trans.*, 2010, **39**, 8153-8160.

[19] T. K. Macklin, V. Sniekus, *Org. Lett.*, 2005, **7**, 2519-2522.
[20] D. A. Malyshev, N. M. Scott, N. Marion, E. D. Stevens, V. P. Ananikov, I. P. Beletskaya, S. P. Nolan, *Organometallics*, 2006, **25**, 4462-4470.
[21] W. Buchowicz, W. Wojtczak, A. Pietrzykowski, A. Lupa, L. B. Jerzykiewicz, A. Makal, K. Woźniak, *Eur. J. Inorg. Chem.*, 2010, 648-656.
[22] A. R. Martin, Y. Makida, S. Meiries, A. M. Z. Slawin, S. P. Nolan, *Organometallics*, 2013, **32**, 6265-6270.
[23] M. Henrion, M. J. Chetcuti, V. Ritleng, *Chem. Commun.*, 2014, **50**, 4624-4627.
[24] R. A. Kelly III, N. M. Scott, S. Díez-González, E. D. Stevens, S. P. Nolan, *Organometallics*, 2005, **24**, 3442-3447.
[25] O. R. Luca, B. A. Thompson, M. K. Takase, R. H. Crabtree, *J. Organomet. Chem.*, 2013, **730**, 79-83.
[26] O. R. Luca, D. L. Huang, M. K. Takase, R. H. Crabtree, *New. J. Chem.*, 2013, **37**, 3402-3405.
[27] F. E. Hahn, M. C. Jahnke, *Angew. Chem. Int. Ed.*, 2008, **47**, 3122-3172.
[28] A. M. Oertel, V. Ritleng, A. Busiah, L. F. Veiros, M. J. Chetcuti, *Organometallics*, 2011, **30**, 6495-6498.
[29] A. M. Oertel, J. Freudenreich, J. Gein, V. Ritleng, L. F. Veiros, M. J. Chetcuti, *Organometallics*, 2011, **30**, 3400-3411.
[30] F. P. Malan, E. Singleton, P. H. van Rooyen, M. Landman, *J. Organomet. Chem.*, 2016, **813**, 7-14.
[31] F. P. Malan, E. Singleton, B. Bulling, I. Cukrowski, P. H. van Rooyen, M. Landman, *Mol. Catal.*, 2017, **432C**, 47-56.
[32] R. J. Errington, *Advanced Practical Inorganic and Metalorganic Chemistry*, Blackie Academic & Professional, London, 1997.
[33] D.F. Shriver, M.A. Drezdzon, *The Manipulation of Air-Sensitive Compounds*, 2nd ed., Wiley, New York, 1986.
[34] D. A. Skoog, D. M. West, F. J. Holler, Fundamentals of Analytical Chemistry (7th edition), Saunders College Publishing, Fort Worth, 1991, p. 468-469.
[35] A. D. Becke, *J. Chem. Phys.*, 1993, **98**, 5648-5652.
[36] C. Lee, W. Yang, R. G. Parr, *Phys. Rev. B.*, 1988, **37**, 785-789.
[37] M. J. Frisch, G. W. Trucks, H. B. Schlegel, G. E. Scuseria, M. A. Robb, J. R. Cheeseman, G. Scalmani, V. Barone, B. Mennucci, G. A. Petersson, H. Nakatsuji, M. Caricato, X. Li, H. P. Hratchian, A. F. Izmaylov, J. Bloino, G. Zheng, J. L. Sonnenberg, M. Hada, M. Ehara, K. Toyota, R. Fukuda, J. Hasegawa, M. Ishida, T. Nakajima, Y. Honda, O. Kitao, H. Nakai, T. Vreven, J. A. Montgomery (Jr), J. E. Peralta, F. Ogliaro, M. Bearpark, J. J. Heyd, E. Brothers, K. N. Kudin, V. N. Staroverov, T. Keith, R. Kobayashi, J. Normand, K. Raghavachari, A. Rendell, J. C. Burant, S. S. Iyengar, J. Tomasi, M. Cossi, N. Rega, J. M. Millam, M. Klene, J. E. Knox, J. B. Cross, V. Bakken, C. Adamo, J. Jaramillo, R. Gomperts, R. E. Stratmann, O. Yazyev, A. J. Austin, R. Cammi, C. Pomelli, J. W. Ochterski, R. L. Martin, K. Morokuma, V. G. Zakrzewski, G. A. Voth, P. Salvador, J. J. Dannenberg, S. Dapprich, A. D. Daniels, O. Farkas, J. B. Foresman, J. V. Ortiz, J. Cioslowski, D. J. Fox, Gaussian 09, Revision D.01, Gaussian Inc., Wallingford CT, 2010.
[38] F. Weigend, R. Ahlrichs, *Phys. Chem. Chem. Phys.*, 2005, **7**, 3297-3305.
[39] J. W. McIver, A. K. Komornicki, *J. Am. Chem. Soc.*, 1972, **94**, 2625-2633.
[40] J. H. Tocher, D. I. Edwards, *Free Rad. Res. Comms.*, 1987, **4**, 269-276.
[41] A. Kuhn, K. G. von Eschwege, J. Conradie, *J. Phys. Org. Chem.*, 2012, **25**, 58-68.
[42] M. J. Cook, I. Chambrier, G. F. White, E. Fourie, J. C. Swarts, *Dalton Transactions*, 2009, **7**, 1136-1144.
[43] R.S. Nicholson, I. Shain, *Analytical Chemistry*, 1964, **36**, 706-723.
[44] P. R. Wells, *Progress in Physical Organic Chemistry*, John Wiley & Sons Inc., New York, 1968, 6, 111-145.
[45] R. E. Kagarise, *J. Am. Chem. Soc.*, 1955, **47**, 1377–1379.
[46] R. Li, X. Zhang, P. Zhu, D. K. P. Ng, N. Kobayashi, J. Jiang, *Inorg. Chem.*, 2006, **45**, 2327-2334.
[47] C. Heinemann, T. Muller, Y. Apeloig, H. Schwarz, *J. Am. Chem. Soc.*, 1996, **118**, 2023-2038.
[48] C. Boehme, G. Frenking, *J. Am. Chem. Soc.*, 1996, **118**, 2039-2046.

[49] J. F. Lehmann, S. G. Urquhart, L. E. Ennis, A. P. Hitchcock, K. Hatano, S. Gupta, M. K. Denk, *Organometallics*, 1999, **18**, 1862-1872.
[50] (a) D. H. McDaniel, H. C. Brown, *J. Org. Chem.*, 1958, **23**, 420-427. (b) C. Hansch, A. Leo, R. W. Taft, *Chem. Rev.*, 1991, **91**, 165-195.
[51] J. Conradie, *J. Chem. Soc., Dalt. Trans.*, 2015, **44**, 1503–1515.
[52] J. D. L. Holloway, W. E. Geiger, Jr., *J. Am. Chem. Soc.*, 1979, **101**, 2038-2044.
[53] S. P. Gubin, S. A. Smirnova, L. I. Denisovich, *J. Organomet. Chem.*, 1971, **30**, 257-265.
[54] S. K. Ritter, *Chemical & Engineering News*, 2016, **94**, 6-6.
[55] J. Ferrando-Soria, O. Fabelo, M. Castellano, J. Cano, S. Fordham, H-C. Zhou, *Chem. Commun.*, 2015, **51**, 13381-13384.
[56] S. Thangavel, S. Boopathi, N. Mahadevaiah, P. Kolandaivel, P. B. Pansuriya, H. B. Friedrich, *J. Mol. Catal. A.*, 2016, **423**, 160-171.
[57] J. P. Perdew, M. Levy, *Physical Review B.*, 1997, **56**, 16021-16028.
[58] U. Salzner, R. Baer, *J. Chem. Phys.*, 2009, **131**, 231101.
[59] M. M. Rogers, S. S. Stahl, *Topics in Organometallic Chemistry*, Springer, 2006, **21**, 21-46.